C0 and C1 N-terminal Ig domains of myosin binding protein C exert different effects on thin filament activation

Samantha P. Harris[a], Betty Belknap[b], Robert E. Van Sciver[b], Howard D. White[b], and Vitold E. Galkin[b,1]

[a]Department of Cellular and Molecular Medicine, University of Arizona, Tucson, AZ 85724; and [b]Department of Physiological Sciences, Eastern Virginia Medical School, Norfolk, VA 23507

Edited by J. G. Seidman, Harvard Medical School, Boston, MA, and approved January 8, 2016 (received for review September 22, 2015)

Mutations in genes encoding myosin, the molecular motor that powers cardiac muscle contraction, and its accessory protein, cardiac myosin binding protein C (cMyBP-C), are the two most common causes of hypertrophic cardiomyopathy (HCM). Recent studies established that the N-terminal domains (NTDs) of cMyBP-C (e.g., C0, C1, M, and C2) can bind to and activate or inhibit the thin filament (TF). However, the molecular mechanism(s) by which NTDs modulate interaction of myosin with the TF remains unknown and the contribution of each individual NTD to TF activation/inhibition is unclear. Here we used an integrated structure–function approach using cryoelectron microscopy, biochemical kinetics, and force measurements to reveal how the first two Ig-like domains of cMyPB-C (C0 and C1) interact with the TF. Results demonstrate that despite being structural homologs, C0 and C1 exhibit different patterns of binding on the surface of F-actin. Importantly, C1 but not C0 binds in a position to activate the TF by shifting tropomyosin (Tm) to the "open" structural state. We further show that C1 directly interacts with Tm and traps Tm in the open position on the surface of F-actin. Both C0 and C1 compete with myosin subfragment 1 for binding to F-actin and effectively inhibit actomyosin interactions when present at high ratios of NTDs to F-actin. Finally, we show that in contracting sarcomeres, the activating effect of C1 is apparent only once low levels of Ca^{2+} have been achieved. We suggest that Ca^{2+} modulates the interaction of cMyBP-C with the TF in the sarcomere.

muscle regulation | cryo-EM | myosin binding protein C | actin | tropomyosin

Intense interest in cardiac myosin binding protein C (cMyBP-C) has followed the initial discovery that cMyBP-C mutations are linked to hypertrophic cardiomyopathy (HCM) (1, 2). Mutations in the gene encoding cMyBP-C and altered posttranslational modifications of cMyBP-C are linked to HCM and heart failure (3, 4). Accordingly, recent studies revealed that cMyBP-C is a significant regulator of cardiac contraction under normal physiological conditions where it is required to ensure proper timing between force activation and relaxation (5) and prolongs the time course of systolic ejection (6, 7). The primary sequence of mammalian cMyBP-C indicates that it is composed of eight Ig- and three fibronectin (Fn)-like domains (Fig. 1, *Inset*). The first four N-terminal domains (NTDs) C0, C1, C2, and the regulatory M-domain, bind to F-actin (8, 9) and/or to myosin S2 (10), whereas C-terminal domains C7–C10 bind to nine locations on each half of the myosin thick filament (11). Electron tomography of muscle sections revealed that MyBP-C directly links thick and thin filaments in muscle sarcomeres, demonstrating the physiological relevance of these interactions (12).

Previously, only two mechanisms were known to activate cardiac muscle contraction: binding of calcium to troponin and binding of strongly bound myosin cross-bridges to the thin filament (TF) (13). However, recent studies established that the NTDs of cMyBP-C can also potently activate or inhibit the TF (14–16). Electron microscopy (EM) studies of negatively stained TFs decorated with NTDs of cMyBP-C including C0-C1-M-C2 confirmed the ability of NTDs to shift tropomyosin (Tm) and activate the TF (17). Nevertheless, the underlying mechanism(s) of the activation/inhibition of the TF by the NTDs of cMyBP-C still remain uncertain because the contribution of the individual domains (e.g., C0, C1, PA, M, and C2) to this process is unclear. Motility assays demonstrated that both the C1 domain and the PA-linker, but not the C0 domain, of the human cMyBP-C contribute to the TF activation (18). However, EM of negatively stained decorated actin filaments (19) suggested that C0 and C1 Ig domains could each bind to the same position on F-actin and potentially activate the TF by means of forcing Tm to move into its "open" position, thus exposing myosin binding sites along the actin filament. In this study, we used a combined approach of cryo EM, steady-state ATP hydrolysis assay, and force measurements in permeabilized myocytes to define the structure/function relationships of the individual C0 and C1 Ig-like domains of human cMyBP-C with native cardiac TFs. We unambiguously show that C0 and C1, two structurally homologous Ig-like domains, each bind to F-actin in a very distinct fashion and exert different effects on the activation state of the TF. We demonstrate that C1, but not C0, can activate the TF by shifting the Tm cable to the open structural state. Importantly, we demonstrate that only the C1 domain can directly interact with the Tm and trap the Tm cable in the open position. Finally, we show that C1 but not C0 increases Ca^{2+} sensitivity of force in permeabilized muscle and that effects of C1 to augment force become evident at low levels of activating Ca^{2+}. We suggest that Ca^{2+} may modulate the interaction of cMyBP-C with the TF by "loosening" the Tm cable on the surface of F-actin and allowing cMyBP-C NTDs to bind the TF.

Significance

Cardiac myosin binding protein C (cMyBP-C) is a regulatory protein that modulates the strength and speed of heart contractions. cMyBP-C is required for normal heart function, and mutations in the gene encoding cMyBP-C are the most common cause of hypertrophic cardiomyopathy, a disease affecting an estimated 1 in 500 people. Here we used an integrated structure–function approach to determine how C0 and C1, the first two domains of cMyBP-C, interact with muscle thin filaments (composed of F-actin and regulatory proteins) to influence their ability to interact with myosin, the force-generating protein of muscle. Results reveal that C0 and C1 both bind to actin at multiple, distinct sites and that C0 and C1 exert different effects on heart muscle contraction.

Author contributions: S.P.H., H.D.W., and V.E.G. designed research; S.P.H., B.B., R.E.V.S., and V.E.G. performed research; S.P.H., H.D.W., and V.E.G. analyzed data; and S.P.H., H.D.W., and V.E.G. wrote the paper.

The authors declare no conflict of interest.

This article is a PNAS Direct Submission.

[1]To whom correspondence should be addressed. Email: galkinve@evms.edu.

This article contains supporting information online at www.pnas.org/lookup/suppl/doi:10.1073/pnas.1518891113/-/DCSupplemental.

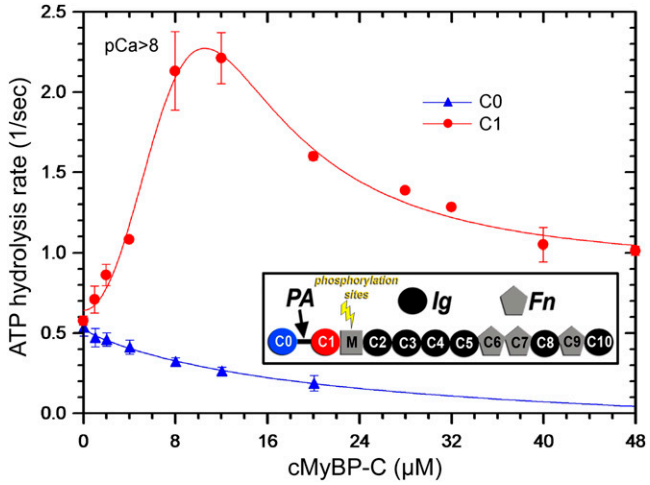

Fig. 1. Effects of C0 and C1 on TF-dependent myosin-S1 ATPase activity. Data in the presence of C0 was fit by a simple inhibition equation $V(C0) = Vo/(1+ ([C0]/K_{iC0}))$, where $K_{i\ c0} = 12.1 \pm 1$ μM, whereas data in the presence of C1 shows cooperative activation and inhibition that yields a best fit using $V(C1) = V_1/(1 + (K_m/[C1])^n + ([C1]/K_i)^n) + V_o$ equation, where $V_1 = 3.2 \pm 0.3 \cdot s^{-1}$, $K_m = 8.4 \pm 1$ μM, $K_i = 15.2 \pm 3$ μM, and $n = 2.1 \pm 0.3$ and $V_o = 0.6 \pm 0.1 \cdot s^{-1}$. Final protein concentrations used were 0.65 μM S1 and 5 μM TFs. Domain structure of the NTD of cMyBP-C is shown in the *Inset*.

Results

C0 and C1 Ig Domains of cMyBP-C Exert Differential Effects on TF Activation of ATP Hydrolysis by Myosin Subfragment 1. The goal of this study was to systematically compare the activating and inhibitory effects of C0 and C1 (Fig. 1), to determine whether effects of these domains were unique or redundant, and to determine structural elements that are essential for their function. We first used high-speed cosedimentation binding assays to measure the binding affinity of each domain for native cardiac TFs and F-actin (*SI Appendix*, Fig. S1 *C* and *D*). Although C0 and C1 bind to TFs and F-actin with similar affinities, only C1 binding to TFs is cooperative. K_ds for each domain were comparable although somewhat lower that those determined for multidomain fragments under similar conditions (9), suggesting a cumulative contribution of the individual domains to the overall affinity of the larger cMyBP-C fragments.

It has previously been shown that the C0-C1 NTDs of human cMyBP-C can activate the TF in the absence of Ca^{2+} (18). We therefore next used steady-state ATPase measurements to determine if either of the individual C0 or C1 domains could activate the TF under Ca^{2+}-free conditions. As shown in Fig. 1, C0 and C1 had dramatically different effects on TF-activated rates of myosin-subfragment 1 (S1) ATP hydrolysis. Whereas C0 inhibited TF activation of myosin-S1 ATP hydrolysis, C1 exerted a concentration-dependent biphasic effect on the activation state of the TF with maximal activation at ∼10 μM. Higher concentrations of C1 then reduced TF activation of myosin-S1 ATP hydrolysis. Therefore, our biochemical experiments confirm previous observations (18) that human C0 alone does not activate the TF and is consistent with the conclusion that C1 contributes to activation of the actomyosin interactions in the absence of Ca^{2+} ions (18).

C0 Does Not Interfere with Tm on the Surface of F-Actin, but Can Compete with Myosin-S1 Binding to Actin. To determine the structural basis for differences in the activating and inhibitory effects of C0 and C1, we next used cryoelectron microscopy (cryo-EM) to identify whether each domain occupies unique binding sites on the TF. To first identify the binding site of C0 on the surface of TF, we performed 3D reconstructions of frozen hydrated TFs decorated with the C0 fragment (*SI Appendix*, Fig. S2*A*) using a single particle approach (20). The single particle approach permits sorting of individual filament segments into structural classes based on their occupancy and structural modes. A caveat to the cryo-EM approach, however, is that upon freezing, some proteins may be stripped off TFs. Consistent with this possibility, cross-correlation sorting revealed that ∼45% of TF segments analyzed were naked F-actin that lacked regulatory proteins (*SI Appendix*, *SI Materials and Methods*). These naked segments were therefore excluded from subsequent sorting procedures and analysis.

Six structural classes were identified within C0-decorated TF segments, and their 3D reconstructions are shown in Fig. 2 *A*–*F*. Greater than 60% of the occupied segments had C0 attached to F-actin but were missing Tm (Fig. 2 *A*–*C*), whereas 17% of segments had Tm attached to F-actin but had no C0 domain bound (Fig. 2*D*). We examined the position of the Tm in these

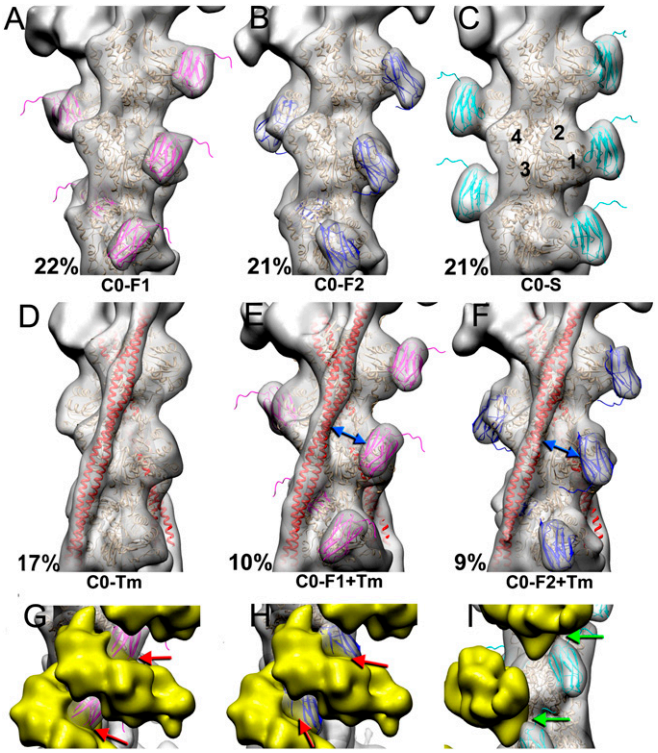

Fig. 2. The C0 Ig-like domain of cMyBP-C binds to three distinct sites on the surface of actin filaments and does not interfere with the closed position of the Tm on F-actin. Reconstructions are shown as gray transparent surfaces. The frequency of each structural mode is denoted on the left of each map. Actin molecules are shown as tan ribbons, Tm is shown as red ribbons, and the NMR structure of the C0 Ig domain (PDB: 2K1M) is shown in magenta (C0-F1 mode), blue (C0-F2 mode), or cyan (C0-S mode). Actin subdomains are numbered in black. (*A*–*C*) Three-dimensional reconstructions of structural classes of TF segments that have Tm stripped off, but are uniformly decorated with C0. C0 binds to the front of F-actin in two structural modes indicated as C0-F1 (*A*) and C0-F2 (*B*). C0 also binds to the side of F-actin, denoted here as C0-S mode (*C*). (*D*) Three-dimensional reconstruction of TF segments uniformly occupied with Tm, but not with the C0 domain, shows Tm (red ribbons) in the closed position (21). (*E* and *F*) Three-dimensional reconstructions of TF segments uniformly occupied with Tm (red ribbons) and possessing C0 domain bound in either C0-F1 (*E*) or C0-F2 (*F*) modes. C0 in both structural modes is distal from the Tm in the closed position (blue arrows). (*G*–*I*) Projected position of the S1 myosin head on the surface of F-actin (solid yellow) (24) clashes with C0 in either C0-F1 (*G*) or C0-F2 (*H*) modes (red arrows) but has no steric hindrance with C0 in the C0-S mode (*I*, green arrows).

C0-free segments and determined that the Tm was in the "closed" rather than the "blocked" structural state, because the atomic model of Tm–F-actin complex (21) perfectly matched the 3D reconstruction without any perturbations in the position of the Tm cable.

It has been previously shown that C0 can bind to the two sites of the surface of the actin molecule—the "front" and the "side" sites (19). We found both modes of binding in the frozen hydrated C0-decorated actin filaments (Fig. 2 *A*–*C*). However, the overall reconstruction of the front mode did not match the NMR structure of C0 [Protein Data Bank (PDB): 2K1M] (*SI Appendix*, Fig. S3). Subsequent particle sorting resolved the discrepancy by revealing that C0 binds to the front of the actin molecule in two structural modes (Fig. 2 *A* and *B*, respectively), related by ∼125° in-plane rotation (*SI Appendix*, Fig. S4*A*). We denote these two modes of binding here as C0 front mode 1 (C0-F1) and C0 front mode 2 (C0-F2).

At a resolution of ∼15 Å (*SI Appendix*, Fig. S9), we were able to unambiguously dock the NMR structure of C0 (PDB: 2K1M) into the two 3D reconstructions of these two front modes (C0-F1 and C0-F2) to determine which residues of C0 may be involved in the interaction with F-actin (*SI Appendix*, Fig. S4). Our data suggest that the transition between the two front modes of C0 binding may be a rotation around the flexible hinge composed of the N terminus of actin and the 37–54 loop of the C0 domain (*SI Appendix*, Fig. S4). Particle sorting further revealed an additional mode of interaction of C0 with F-actin, which we call side mode and denote as C0-S in (Fig. 2*C*). Interestingly, the 37–54 loop of the C0 Ig domain is involved in all of the three modes of interaction of the C0 domain with F-actin (C0-F1, C0-F2, and C0-S), and therefore is the main determinant in the interaction of C0 with the TF (*SI Appendix*, Fig. S4 *B*–*D*). In our pseudoatomic models, C0 residues 42, 49, 80, 81, and 83 are predicted to interact with F-actin, in good agreement with previous results by NMR (22). Therefore, our cryo-EM data are in excellent agreement with NMR spectroscopy.

We did not find any TF segments uniformly decorated with C0 bound to F-actin solely in the side mode (Fig. 2*C*), but we were able to isolate segments of TFs decorated with C0 in the two front modes (Fig. 2 *E* and *F*). In the reconstructions of C0-F1 + Tm and C0-F2 + Tm, the position of the C0 on the surface of F-actin was indistinguishable from C0-F1 and C0-F2 classes where Tm was absent (compare Fig. 2 *A* and B with *E* and *F*). Our cryo-EM data unambiguously demonstrate that in either of the C0-F1 + Tm and C0-F2 + Tm modes, the C0 domain of cMyPB-C is bound distantly from the Tm in the closed state (Fig. 2 *E* and *F*, blue arrows). To evaluate whether C0 may interfere with the Tm in the blocked structural state (23) we superimposed Tm cable in the blocked position onto our 3D reconstructions of TF decorated with C0 Ig domain (*SI Appendix*, Fig. S5 *A* and *B*). Our data indicate that the C0 will not interfere with Tm in the blocked state, because in either front binding mode (e.g., C0-F1 and C0-F2) C0 is distal from Tm. This observation is consistent with the lack of TF activation by C0 in ATPase assays at pCa > 8 (Fig. 1, blue curve). At the same time, in either front binding mode, C0 could compete with actomyosin interactions because its position on the surface of F-actin overlaps with the binding site of myosin S1 (Fig. 2 *G* and *H*, red arrows). In contrast, C0 bound in the side mode does not clash with myosin S1 (Fig. 2*I*, green arrows). Because >60% of actin-decorated segments showed C0 in one of the front modes, cryo-EM data are consistent with C0 inhibition of myosin-S1 TF-dependent ATP hydrolysis at high ratios of C0 to myosin S1 (Fig. 1, blue curve). To summarize, cryo-EM data demonstrate that C0 of human cMyBP-C cannot activate the TF.

C1 Activates the TF by Trapping Tm in the Open State on the Surface of F-Actin. Next, we sought to identify the binding site(s) of C1 on the surface of the TF. We performed 3D reconstructions of frozen hydrated TFs decorated with C1 (*SI Appendix*, Fig. S2*B*) using a single particle approach as described for C0. Cross-correlation sorting revealed that ∼31% of segments were naked F-actin, which were excluded from the following sorting procedure as described above for C0.

Six structural classes for C1 were found within the decorated segments and their 3D reconstructions are shown in Fig. 3. Approximately 60% of the occupied segments had C1 attached to F-actin but were missing Tm (Fig. 3 *A*–*C*), whereas 14% of segments had Tm attached to F-actin but had no C1 domain bound (Fig. 3*D*). Despite the low Ca^{2+} conditions, the position of the Tm in these C1-free segments perfectly matched the open state of the Tm (24), suggesting that C1 alone can activate the TF in a cooperative manner similar to the rigor state of myosin S1.

In decorated frozen hydrated TFs, C1 was found to bind to two sites on the surface of the actin filament called front and side modes (Fig. 3 *A*–*C*, *E*, and *F*). First, isolated segments were identified that had Tm stripped off, but showed C1 decoration. We did not find any segments with C1 bound in the side mode within those segments because all of the segments had C1 bound to F-actin in the front mode. The overall reconstruction of the C1 front class did not match the crystal structure of the C1 Ig domain (25), but subsequent sorting revealed that C1 binds to the front of the actin molecule in three structural modes (Fig. 3 *A*–*C*), which we denote here as C1 front mode 1 (C1-F1), C1 front mode 2 (C1-F2), and C1 front mode 3 (C1-F3). At a resolution of ∼15 Å (*SI Appendix*, Fig. S10) we were able to unambiguously dock the crystal structure of C1 (PDB: 2V6H) (25) into all three 3D reconstructions of these front modes, allowing us to determine which residues of C1 Ig domain may be involved in the interaction with F-actin (*SI Appendix*, Fig. S6 *A*–*C*). Our data indicate that the three front modes are structurally related and may represent different stages of interaction of C1 with F-actin (*SI Appendix*, Fig. S6).

To reveal how C1 binding can activate the TF under low Ca^{2+} conditions (Fig. 1, red curve) we looked for TF segments decorated with both C1 and Tm. Interestingly, the only front class of segments that contained Tm had C1 bound in the C1-F1 mode (Fig. 3*E*, blue ribbons). To evaluate whether C1 bound to the TF in the other front modes could also shift Tm to the open position, we imposed the closed structural state of Tm (21) onto all of the three C1 front modes (Fig. 3 *H*–*J*, red ribbon and red surface). In C1-F1 and C1-F2 modes, there were no clashes between the C1 and Tm in the closed state (Fig. 3 *H* and *I*, green arrows). However, C1 bound in the C1-F3 mode clashed with the closed Tm position (Fig. 3*J*, blue arrow). Similarly, when the three front modes were superimposed onto the Tm in the blocked state, all of the front modes yielded an obvious clash with the Tm cable on the surface of F-actin (*SI Appendix*, Fig. S5 *C*–*E*). Therefore, cryo-EM data suggest that C1 in all three front binding modes can shift Tm from either a blocked or closed state toward the open configuration.

The only structural class in which C1 was bound to F-actin in the side mode was fully decorated with Tm (Fig. 3*F*). Moreover, the 3D reconstruction of that class revealed that C1 was directly interacting with the Tm cable, yielding a prominent contact between the C1 and the Tm densities (Fig. 3*F*, red arrows). The residues that are likely to be involved in the interactions of C1 with the Tm and F-actin when C1 is bound in the side mode are shown in *SI Appendix*, Fig. S6. Our structural data are in good agreement with results from NMR, because residues 197, 198, 230, and 242 of C1, which were predicted to interact with actin (22), are located at the interface with F-actin in our pseudoatomic models (*SI Appendix*, Fig. S6*F*). We also show that C1 in any of the front modes may compete with actomyosin interactions (Fig. 4 *K*–*M*), which potentially explains inhibition of the myosin-S1 ATPase activity at high ratios of C1 to myosin S1 (Fig. 1, red curve).

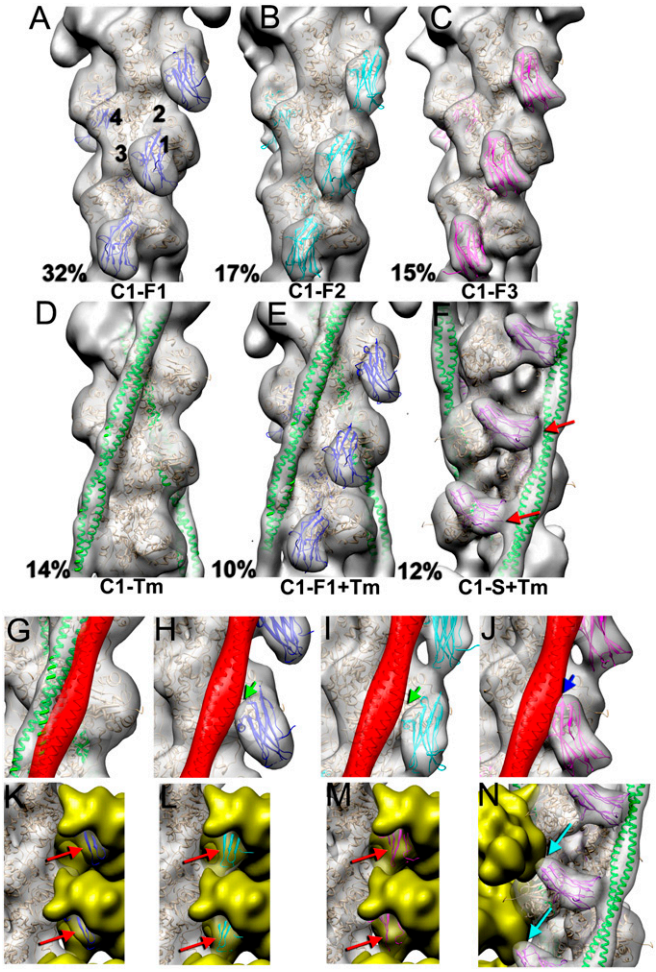

Fig. 3. The C1 Ig-like domain of cMyBP-C displaces Tm from its closed position on F-actin when bound in the front mode and traps Tm in its open state when bound to TF in the side mode. Reconstructions are shown as gray transparent surfaces. The frequency of each structural mode is denoted on the left of each map. Actin molecules are shown as tan ribbons, Tm in the open state is shown as green ribbons, whereas Tm in the closed state is shown as red ribbons and red surface. The crystal structure of the C1 Ig-like domain (PDB: 2V6H) is shown in blue (C1-F1 mode), cyan (C1-F2 mode), magenta (C1-F3 mode), or purple (C1-S mode). Actin subdomains are numbered in black in *A*. All complexes were formed at low Ca^{2+} levels (pCa > 8). (*A–C*) Three-dimensional reconstructions of structural classes of TF segments that have Tm stripped off, but are uniformly decorated with C1. C1 binds to the front of F-actin in three structural modes indicated as C1-F1 (*A*), C1-F2 (*B*), and C1-F3 (*C*). (*D*) Three-dimensional reconstruction of TF segments uniformly occupied with Tm, but not with the C1, show Tm (green ribbons) in the open position on the surface of F-actin (24). (*E* and *F*) Three-dimensional reconstructions of TF segments uniformly occupied with Tm (green ribbons) and possessing C1 bound in either C1-F1 (*E*) or side (*F*) modes. Importantly, in the side mode (C1-S + Tm) C1 makes a prominent contact with Tm (*F*, red arrows). (*G*) Both open (green ribbons) and closed (red ribbons and red surface) positions of Tm on F-actin are shown. (*H* and *I*) Wheres C1 bound in C1-F1 (*H*) or C1-F2 (*I*) modes does not clash with the Tm in the closed state (*H* and *I*, green arrows), it collides with Tm when bound in C1-F3 mode (*J*, blue arrow). (*K–N*) In all three front modes, C1 interferes with the actomyosin interaction (*K–M*, red arrows), but is not projected to have steric clashes with myosin heads when bound in side mode (*N*, cyan arrows).

C1 but Not C0 Increases Ca^{2+} Sensitivity of Force in Contracting Sarcomeres. Because both cryo-EM and ATPase assays were performed in vitro with isolated proteins under conditions of relatively low ionic strength (~50 mM), we next sought to determine whether the activating and inhibitory effects of the individual C0 and C1 domains were evident in contracting sarcomeres under conditions more closely resembling physiological ionic strength (180 mM) and salt composition. We therefore measured passive and active force generation in detergent-permeabilized cardiac myocytes incubated with or without C0 and C1. Previous studies showed that 30–80 μM human or mouse cMyBP-C NTDs could activate force in sarcomeres in the absence of Ca^{2+} (e.g., at pCa 9.0) (16). However, results shown in Fig. 4*A* demonstrate that neither C0 nor C1 at concentrations up to 100 μM had any activating effects on contraction in the absence of Ca^{2+}, i.e., neither C0 or C1 increased passive force in Ca^{2+} solutions at pCa 9. However, in the presence of low [Ca^{2+}], which was not sufficient to significantly activate force (e.g., pCa 5.8, Fig. 4*B*), C1 but not C0 significantly enhanced force generation. C1 thus caused a significant leftward shift of the tension–pCa relationship (Fig. 4*C*) as evident by the reduced calcium concentration required to reach half maximal force generation (i.e., the pCa_{50} for force development was shifted to the left by ~0.31 pCa units (pCa_{50} values were 5.58 ± 0.033 and 5.89 ± 0.072 in the absence and presence of 100 μM C1, respectively). Maximal force generation at saturating Ca^{2+} (e.g., at pCa 4.5) was not significantly affected by either C0 or C1 (Fig. 4*B*). Taken together, results from force generation in permeabilized myocytes are consistent with our data showing activating effects of C1 on TF-stimulated myosin ATPase activity and cryo-EM data showing that C1 can influence the position of the TM cable and trap it in an open state. However, results in permeabilized myocytes under conditions that more closely approach physiological ionic strength and composition suggest that C1 alone is not sufficient to shift the position of Tm to activate force in sarcomeres. Activating effects of C1 on force may thus require

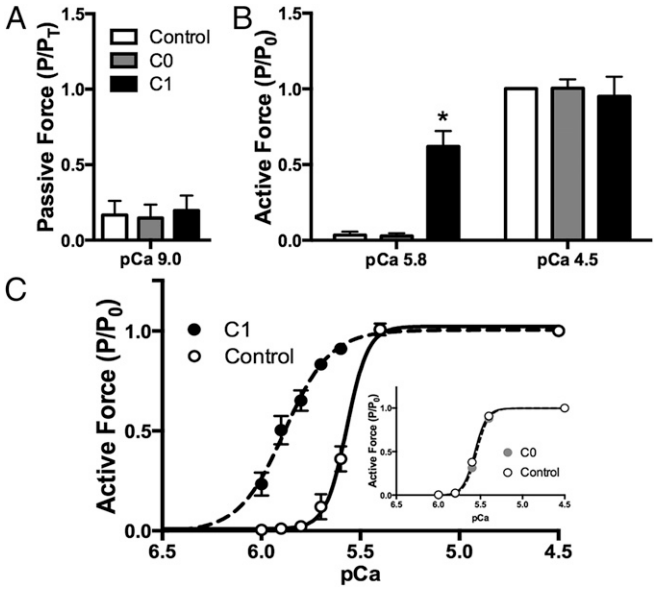

Fig. 4. Effects of C0 and C1 on passive and Ca^{2+}-activated force in permeabilized myocytes. (*A*) C0 (gray) and C1 (black) (100 μM) did not affect passive force in the absence of Ca^{2+} (pCa 9.0). Passive force at pCa 9.0 was expressed as a fraction of total force (P_T, where P_T = total maximal active and passive force measured at pCa 4.5). (*B*) Relative Ca^{2+}-activated force measured in solutions of low Ca^{2+} (pCa 5.8) and maximal activating Ca^{2+} (pCa 4.5). Active forces (P) are expressed normalized to maximal active force at pCa 4.5 (P_0, where $P_0 = P_T - P_{9.0}$) under control conditions in the absence of C0 or C1 (open bar). C0 had no effect on force at either pCa 5.8 or pCa 4.5, whereas C1 increased force measured at pCa 5.8. (*C*) Summary tension–pCa relationships before and after addition of 100 μM C0 or C1. C1 significantly increased myofilament Ca^{2+} sensitivity of tension [pCa_{50} values before and after C1 were 5.58 ± 0.033 and 5.89 ± 0.072 (n = 5), respectively]. (*Inset*) C0 had no effect on myofilament Ca^{2+} sensitivity of tension [pCa_{50} values before and after C0 were 5.57 ± 0.027 and 5.54 ± 0.030 (n = 5), respectively].

additional contributions from other cMyBP-C NTDs in the absence of Ca^{2+} or may only become apparent after low levels of activating Ca^{2+} are achieved.

Discussion

Although it is commonly accepted that cMyBP-C can act as a "brake" to slow cross-bridge interactions (26, 27), until recently most explanations for the effects of cMyBP-C focused exclusively on the ability of cMyBP-C to bind to the thick filament and restrict the ability of myosin S1 heads to bind actin and produce force or motion (27, 28). However, despite the widespread appeal of this idea, evidence that cMyBP-C limits the mobility of myosin heads via interactions with the thick filaments is still lacking. In contrast, we and others have shown that the NTDs of the cMyBP-C (e.g., C0, PA, C1, M, and C2) can bind to the TF and potently activate actomyosin interactions (14, 16, 29, 30). The precise mechanism(s) by which cMyBP-C affects contraction is still unresolved, in part because there is a lack of understanding of how individual domains of cMyPB-C contribute to the overall effects of this multidomain protein on muscle contraction.

In this study, we aimed to fully characterize the interaction of the first two individual NTDs of human cMyPB-C with the native cardiac TF. Previously, both the C0 and C1 Ig-like domains of cMyPB-C were shown to interact with F-actin polymorphically with the ability of each domain to bind to the same two different positions on F-actin called front and side modes (19). Here we confirm that both C0 and C1 can bind to the two positions on the surface of the actin filament (Figs. 2 and 3), but in contrast to previous observations, we show that the binding modes of C0 and C1 to F-actin are very different. The difference in the positioning of the C0 and C1 domains on the surface of F-actin between our study and the previously published work (19) may be attributed in part to differences in sample preparation. For instance, we used frozen hydrated filaments, whereas Orlova et al. (19) used negative staining. It is well accepted that negative staining can introduce flattening of actin filaments upon sample preparation, which in turn may lead to dislocation of actin binding proteins from their putative binding site of F-actin. Therefore, it is possible that our structural data obtained using the cryo-EM approach reveals subtle details of interaction of both C0 and C1 domains with F-actin that cannot be visualized with other standard approaches.

It has been proposed that the absence of C0 in skeletal muscle can be explained by redundancy in the interaction of the first two Ig domains with F-actin (19). However, our data demonstrate that C0 and C1 are not functionally redundant and thus argue against this possibility. That is, C1 efficiently activates actomyosin interactions, whereas C0 does not (Fig. 1). What then might be a functional role of C0 that is unique to cardiac muscle? In our recent paper (9), we showed that the C0-PA-C1-M-C2 fragment is more potent at activating the TF than the C1-M-C2 fragment, suggesting that C0 (or C0-PA) contributes to cMyBP-C TF activation. One possibility is that if C0 cannot activate the TF on its own, it may act to enhance the overall affinity of the N terminus of cMyBP-C for actin by adding an additional contact with the TF. For instance, in the side mode, C0 may work as a cross-linker that does not interfere with the actomyosin interactions (Fig. 2*I*), but maintains C1, M, and C2 domains of cMyBP-C NTD in close proximity to the front of the actin filament where they may contribute (14, 15) to the activation of the TF. Another possibility is that C0 may contribute to regulation of cardiac muscle contraction through inhibition of actomyosin interactions. For instance, our structural data indicate that both C0-F1 and C0-F2 front modes compete with myosin for interaction with F-actin and therefore could inhibit myosin ATPase activity (Fig. 1, blue curve). However, because we found that C0 does not inhibit force generation in permeabilized myocytes, it remains to be determined whether the inhibitory effects of C0 require the presence of additional flanking domains such as the proline–alanine-rich (PA) linker in contracting sarcomeres.

Our data provide a plausible mechanism of how C1 directly activates the TF at low Ca^{2+} conditions. The initial binding of the C1 to the front site, either in the absence of Ca^{2+} (Fig. 1) or at low Ca^{2+} (Fig. 4*B*), shifts Tm from either the blocked (*SI Appendix*, Fig. S5 *C–E*) or closed (Fig. 3*J*) state to the open position. This movement of the Tm toward subdomain 4 of F-actin permits interaction of C1 bound in the side mode with Tm (Fig. 3*F*), which in turn stabilizes the Tm in the open structural state and therefore activates the TF in a manner similar to myosin S1 bound in the rigor state. This finding is consistent with conclusions from a recent study where we suggested that low concentrations of NTDs of cMyBP-C activate the TF by a mechanism similar to that of rigor myosin S1 (9).

To provide insight into how C0 and C1 may bind to F-actin in the context of the whole NTD, we superimposed the positions of C0 and C1 on F-actin (*SI Appendix*, Fig. S7). Data indicate that both domains cannot bind simultaneously to the front or to the side sites of the same actin protomer due to steric clashes (*SI Appendix*, Fig. S7 *A* and *B*, red arrows). Therefore, C0 and C1 can only bind simultaneously to a single actin protomer when one domain is bound in the front mode, while the other is in the side mode (*SI Appendix*, Fig. S7*C*). Further experiments should reveal how multiple NTDs communicate with adjacent domains and regulatory linkers upon binding to the surface of the TF.

Our results are also in agreement with a study using NTDs from murine cMyBP-C that were shown to activate the TF at low Ca^{2+} by shifting the Tm cable from the blocked to the closed structural state (17). However, in our 3D reconstruction of TFs at low Ca^{2+} conditions, we found the Tm cable to be in the closed rather than blocked state (Fig. 2*D*, red ribbons). Differences between the two studies could be accounted for by differences in negative staining and cryo-EM methods that may lead to differences in the absolute position of the TM cable as previously reported (21). On the other hand, we cannot completely exclude an alternative explanation, which is that the Tn complex may partially strip off from the TF upon sample freezing, leaving the Tm cable in the closed structural state. We cannot distinguish between these two possibilities. Nevertheless, our main conclusions regarding the activity of the two Ig-like domains (e.g., C0 and C1) do not depend on initial localization of the Tm at low Ca^{2+} (e.g., blocked or closed state). Human C0 does not interfere with the Tm in either blocked or closed state (*SI Appendix*, Fig. S5 *A* and *B*, blue arrows) and, hence, cannot activate the TF. At the same time, C1 interferes with the Tm in both blocked and closed states (*SI Appendix*, Fig. S5 *C–E*, red arrows) and hence will displace Tm to its open structural state irrespective of the starting position of the Tm.

However, Mun et al. (17) did not observe movement of Tm to the open state upon binding of a construct consisting of murine domains C0-p/a-C1 and a short 15 amino acid sequence of the M domain ("C0C1f"). A possible explanation for the difference between our results and theirs is that we had previously shown (18) that human C1 is able to activate actomyosin interactions in motility assays, whereas mouse C1 cannot. Therefore, human C1 may interact with the TF in a fundamentally different fashion than murine C1. Finally, Mun et al. (17) did not visualize substantial additional mass of the MyBP-C NTDs bound to the TF, which was presumably due to a very low occupancy in the TFs selected for their 3D reconstructions. Such a low occupancy may not be sufficient to shift tropomyosin to the open structural state.

A goal of the current study was to dissect contributions of the individual domains of cMyBP-C to understand the dual activating and inhibitory effects that have been observed in multiple assessments of cMyBP-C function (14–16). We show that polymorphic binding of cMyBP-C domains to the TF combined with the unique functional effects of individual domains can thus

account at least in part for the complex effects of cMyBP-C NTDs to inhibit or activate the TF. Our data provide a solid basis to understanding the cumulative effect of the multiple NTDs on the function of native cMyBP-C in working muscle. It is an intriguing possibility that polymorphic interactions of cMyBP-C NTDs with the TF also allow cMyBP-C to remain bound to the TF in a variety of configurations that do not directly influence actomyosin interactions, whereas other binding configurations may be dynamic and influence Tm position with the rise and fall of Ca^{2+} during the time course of a single cardiac twitch.

Materials and Methods

Detailed methods are provided in *SI Appendix, SI Materials and Methods* and are summarized here.

Proteins and Buffers. Rabbit skeletal muscle tissue was obtained using a protocol approved by the Eastern Virginia Medical School Institional Animal Care and Use Committee (IACUC). Porcine cardiac muscle tissue was obtained from Pel-Freeze (Rogers, Arkansas). Native porcine cardiac thin filaments, C0 (residues 1–100) and C1 (residues 151–258) domains of human cMyBP-C, and the A1 subfraction of rabbit skeletal myosin S1 were prepared as described previously (9). A buffer was used for kinetic, binding, and cryo-EM experiments: 50 mM KAc, 10 mM Mops, 3 mM $MgCl_2$, 1 mM EGTA, pH 7.0.

Kinetic Measurements. ATP hydrolysis rates were determined by colorimetric measurement of phosphate production as described previously (31).

Cryo-EM.

Sample preparation: A total of 1–2 μM TFs in A buffer were incubated with human C0 or C1 constructs (15–20 μM) for 1–2 min.

Three-dimensional reconstruction: Samples (3.5 μL) were applied to lacey carbon grids and vitrified in a Vitrobot Mark IV (FEI, Inc.). Samples were imaged with a Titan Krios at 300 keV using the Falcon 2 direct electron detector. The SPIDER software package (32) was used for image processing, except the CTFFIND3 software (33) was used to determine the defocus values in the micrographs. The EMAN package (34) was used to extract filament images from micrographs. Fourier shell correlation was used to estimate the resolution (*SI Appendix*, Figs. S9 and S10). NMR structure of C0 (PDB: 2K1M), crystal structure of C1 (PDB: 2V6H), and the atomic model of Tm–F-actin complex (21, 24) were used (without perturbations) in a University of California, San Francisco chimera (35) to generate pseudoatomic models of C0- and C1-decorated TFs.

Force Measurements. Force measurements with or without C0 and C1 were performed as previously described with slight modifications (29). Treatment of all animals was in accordance with the National Research Council Guide for the Care and Use of Laboratory Animals using protocols approved by the Institutional Animal Care and Use Committee at University of Arizona. Detailed methods are described in *SI Appendix, SI Materials and Methods*.

ACKNOWLEDGMENTS. We thank Kelly Dryden for assistance with the microscopy (University of Virginia), Dr. Sabine van Dijk for technical assistance (University of Arizona), and Dr. Gunnar Shroeder (Institute of Complex Systems, Forschungszentrum Jülich) for assistance in data analysis. This work was supported in part by NIH R01 HL080367 (to S.P.H.) and American Heart Association Grant in Aid 19910012 (to H.D.W.).

1. Watkins H, et al. (1995) Mutations in the cardiac myosin binding protein-C gene on chromosome 11 cause familial hypertrophic cardiomyopathy. *Nat Genet* 11(4):434–437.
2. Bonne G, et al. (1995) Cardiac myosin binding protein-C gene splice acceptor site mutation is associated with familial hypertrophic cardiomyopathy. *Nat Genet* 11(4):438–440.
3. LeWinter MM, VanBuren P (2005) Sarcomeric proteins in hypertrophied and failing myocardium: An overview. *Heart Fail Rev* 10(3):173–174.
4. van Dijk SJ, et al. (2009) Cardiac myosin-binding protein C mutations and hypertrophic cardiomyopathy: haploinsufficiency, deranged phosphorylation, and cardiomyocyte dysfunction. *Circulation* 119(11):1473–1483.
5. Janssen PM (2010) Kinetics of cardiac muscle contraction and relaxation are linked and determined by properties of the cardiac sarcomere. *Am J Physiol Heart Circ Physiol* 299(4):H1092–H1099.
6. Palmer BM, et al. (2004) Role of cardiac myosin binding protein C in sustaining left ventricular systolic stiffening. *Circ Res* 94(9):1249–1255.
7. Nagayama T, et al. (2007) Control of in vivo left ventricular [correction] contraction/relaxation kinetics by myosin binding protein C: Protein kinase A phosphorylation dependent and independent regulation. *Circulation* 116(21):2399–2408.
8. Shaffer JF, Kensler RW, Harris SP (2009) The myosin-binding protein C motif binds to F-actin in a phosphorylation-sensitive manner. *J Biol Chem* 284(18):12318–12327.
9. Belknap B, Harris SP, White HD (2014) Modulation of thin filament activation of myosin ATP hydrolysis by N-terminal domains of cardiac myosin binding protein-C. *Biochemistry* 53(42):6717–6724.
10. Gruen M, Gautel M (1999) Mutations in beta-myosin S2 that cause familial hypertrophic cardiomyopathy (FHC) abolish the interaction with the regulatory domain of myosin-binding protein-C. *J Mol Biol* 286(3):933–949.
11. Luther PK, et al. (2008) Understanding the organisation and role of myosin binding protein C in normal striated muscle by comparison with MyBP-C knockout cardiac muscle. *J Mol Biol* 384(1):60–72.
12. Luther PK, et al. (2011) Direct visualization of myosin-binding protein C bridging myosin and actin filaments in intact muscle. *Proc Natl Acad Sci USA* 108(28):11423–11428.
13. Gordon AM, Homsher E, Regnier M (2000) Regulation of contraction in striated muscle. *Physiol Rev* 80(2):853–924.
14. Razumova MV, et al. (2006) Effects of the N-terminal domains of myosin binding protein-C in an in vitro motility assay: Evidence for long-lived cross-bridges. *J Biol Chem* 281(47):35846–35854.
15. Razumova MV, Bezold KL, Tu AY, Regnier M, Harris SP (2008) Contribution of the myosin binding protein C motif to functional effects in permeabilized rat trabeculae. *J Gen Physiol* 132(5):575–585.
16. Herron TJ, et al. (2006) Activation of myocardial contraction by the N-terminal domains of myosin binding protein-C. *Circ Res* 98(10):1290–1298.
17. Mun JY, et al. (2014) Myosin-binding protein C displaces tropomyosin to activate cardiac thin filaments and governs their speed by an independent mechanism. *Proc Natl Acad Sci USA* 111(6):2170–2175.
18. Shaffer JF, Wong P, Bezold KL, Harris SP (2010) Functional differences between the N-terminal domains of mouse and human myosin binding protein-C. *J Biomed Biotechnol* 2010:789798.
19. Orlova A, Galkin VE, Jeffries CM, Egelman EH, Trewhella J (2011) The N-terminal domains of myosin binding protein C can bind polymorphically to F-actin. *J Mol Biol* 412(3):379–386.
20. Egelman EH (2000) A robust algorithm for the reconstruction of helical filaments using single-particle methods. *Ultramicroscopy* 85(4):225–234.
21. von der Ecken J, et al. (2015) Structure of the F-actin-tropomyosin complex. *Nature* 519(7541):114–117.
22. Lu Y, Kwan AH, Trewhella J, Jeffries CM (2011) The C0C1 fragment of human cardiac myosin binding protein C has common binding determinants for both actin and myosin. *J Mol Biol* 413(5):908–913.
23. Pirani A, et al. (2006) An atomic model of the thin filament in the relaxed and Ca2+-activated states. *J Mol Biol* 357(3):707–717.
24. Behrmann E, et al. (2012) Structure of the rigor actin-tropomyosin-myosin complex. *Cell* 150(2):327–338.
25. Govada L, et al. (2008) Crystal structure of the C1 domain of cardiac myosin binding protein-C: Implications for hypertrophic cardiomyopathy. *J Mol Biol* 378(2):387–397.
26. Hofmann PA, Hartzell HC, Moss RL (1991) Alterations in Ca2+ sensitive tension due to partial extraction of C-protein from rat skinned cardiac myocytes and rabbit skeletal muscle fibers. *J Gen Physiol* 97(6):1141–1163.
27. Calaghan SC, Trinick J, Knight PJ, White E (2000) A role for C-protein in the regulation of contraction and intracellular Ca2+ in intact rat ventricular myocytes. *J Physiol* 528(Pt 1):151–156.
28. Starr R, Offer G (1978) The interaction of C-protein with heavy meromyosin and subfragment-2. *Biochem J* 171(3):813–816.
29. Bezold KL, Shaffer JF, Khosa JK, Hoye ER, Harris SP (2013) A gain-of-function mutation in the M-domain of cardiac myosin-binding protein-C increases binding to actin. *J Biol Chem* 288(30):21496–21505.
30. Weith A, et al. (2012) Unique single molecule binding of cardiac myosin binding protein-C to actin and phosphorylation-dependent inhibition of actomyosin motility requires 17 amino acids of the motif domain. *J Mol Cell Cardiol* 52(1):219–227.
31. White HD (1982) Special instrumentation and techniques for kinetic studies of contractile systems. *Methods Enzymol* 85 Pt B:698–708.
32. Frank J, Shimkin B, Dowse H (1981) SPIDER: A modular software system for electron image processing. *Ultramicroscopy* 6:343–358.
33. Mindell JA, Grigorieff N (2003) Accurate determination of local defocus and specimen tilt in electron microscopy. *J Struct Biol* 142(3):334–347.
34. Ludtke SJ, Baldwin PR, Chiu W (1999) EMAN: Semiautomated software for high-resolution single-particle reconstructions. *J Struct Biol* 128(1):82–97.
35. Pettersen EF, et al. (2004) UCSF Chimera: A visualization system for exploratory research and analysis. *J Comput Chem* 25(13):1605–1612.